ADVANCED MATERIALS

DOI: 10.1002/adma.200602927

Hierarchically Structured ZnO Film for Dye-Sensitized Solar Cells with Enhanced Energy Conversion Efficiency**

By *Tammy P. Chou*, *Qifeng Zhang*, *Glen E. Fryxell*, and *Guozhong Cao**

The interest in dye-sensitized solar cells has increased due to reduced energy sources and higher energy production costs. For the most part, titania (TiO_2) has been the material of choice for dye-sensitized solar cells and so far have shown to exhibit the highest overall light conversion efficiency ~11 %.[1] However, zinc oxide (ZnO) has recently been explored as an alternative material in dye-sensitized solar cells with great potential.[2] The main reasons for this increase in research surrounding ZnO material include: 1) ZnO having a bandgap similar to that for TiO_2 at 3.2 eV,[3] and 2) ZnO having a much higher electron mobility ~115–155 $cm^2 V^{-1} s^{-1}$[4] than that for anatase titania (TiO_2), which is reported to be ~10^{-5} $cm^2 V^{-1} s^{-1}$.[5] In addition, ZnO has a few advantages as the semiconductor electrode when compared to TiO_2, including 1) simpler tailoring of the nanostructure as compared to TiO_2, and 2) easier modification of the surface structure. These advantages[6] are thought to provide a promising means for improving the solar cell performance of the working electrode in dye-sensitized solar cells.

It was reported[7] that the surface structure, the particle size and shape, and the porosity are all important factors for optimizing the solar cell performance of dye-sensitized solar cells. With ZnO, these factors can easily be tailored through the modification of solution growth and wet-chemical methods to fabricate various nanostructures. In addition, the surface structure and crystallinity of ZnO for dye-sensitized solar cells can be easily modified through the use of aqueous solution methods to increase the surface area.[8] For example, aligned ZnO nanowires can be prepared by electrochemical deposition, VLS or nucleation growth, or thermal evaporation; whereas, the growth of TiO_2 nanowires are less likely to occur and much more difficult to obtain using such solution growth methods.

So far, the highest overall light conversion efficiency obtained for ZnO nanoparticle film has been ~5 %[9] by utilizing additional compression methods for better particle packing. With typical nanoparticle film processing techniques, the highest overall light conversion efficiency obtained for ZnO has been ~1.5 %.[10]

Here, we describe solar cells consisting of ZnO films with primary nanoparticles and secondary colloidal spheres, fabricated by way of solvothermal processing, and compare the overall light conversion efficiency to that of ZnO films fabricated from commercially-available nanoparticles. Figure 1 depicts the hierarchical structure of the ZnO film.[11] It is thought that hierarchically-structured ZnO particles would promote light scattering through the presence of secondary colloidal spheres, thus, enhancing photon absorption to improve the short-circuit current density and the overall light conversion efficiency.

There has been numerous research groups who have achieved higher short-circuit current densities and higher overall light conversion efficiencies by promoting light

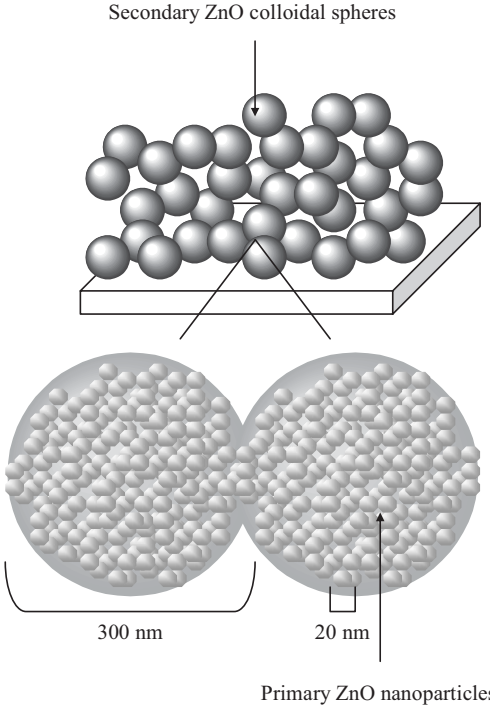

Figure 1. Schematic of the hierarchically-structured ZnO film consisting of secondary ZnO colloids ~300 nm in diameter that are made up of primary ZnO nanoparticles ~20 nm in diameter.

[*] Prof. G. Z. Cao, Dr. T. P. Chou, Dr. Q. Zhang
Department of Materials Science and Engineering
University of Washington
302 Roberts Hall, Box 352120, Seattle, WA 98195 (USA)
E-mail: gzcao@u.washington.edu
Dr. G. E. Fryxell
Institute for Interfacial Catalysis (IIC)
Pacific Northwest National Laboratory (PNNL)
902 Battelle Blvd, Box 999, Richland, WA 99352 (USA)

[**] Financial support by the UW-PNNL Joint Institute for Nanoscience (JIN), jointly funded by the University of Washington (UW) and Pacific Northwest National Laboratory (PNNL, operated by Battelle for the U.S. Department of Energy); the Intel Ph.D. Foundation; and the Air Force Office of Scientific Research (AFOSR-MURI, FA9550-06-1-032). Acknowledgement to Professor Samson Jenekhe and Dr. Abhishek Pradeep Kulkarni for the use of their lab and solar cell equipment.

scattering. For example, it has been reported[12] that the addition of larger SiO_2 or TiO_2 particles with sizes in the micrometer or submicrometer scale into a network of TiO_2 nanoparticles enhanced the scattering of light and thus obtained higher energy conversion efficiencies. In another example, one group reported[13] that the incorporation of a layer of TiO_2 inverse opals[14] into conventional TiO_2 nanoparticle film resulted in an increase in the short-circuit current density by ~26%, which was shown to be mainly due to multiple scattering events.

However, incorporating the TiO_2-SiO_2 system into solar cells would not be favorable since the transparency and insulating behavior of SiO_2 would not be advantageous for photon absorption and electron transport. The addition of SiO_2 would also take up volume, reducing the amount of TiO_2, and would introduce resistance into the TiO_2 film. Furthermore, the conversion efficiencies of TiO_2 inverse opal structures were shown to be low and showed better photovoltaic responses in ordered areas than that in non-ordered areas.[15]

Thus, the hierarchical structure of the ZnO film would be an ideal system to promote light scattering, and to enhance photon absorption for increased electron-hole generation since the hierarchical structure of ZnO with ~300 nm diameter colloidal spheres made up of ~20 nm diameter nanoparticles is assumed to have the same scattering effects with an ordered hierarchical orientation without utilizing two materials.

The crystallinity and crystal size of the hierarchically-structured ZnO films were analyzed using XRD. Figure 2 shows the XRD peaks of ZnO. It can be seen that the ZnO structure is present, showing the (100), (002), (101), and (102) peaks. Using the Scherer equation,[16] the crystal size of the primary nanoparticles was estimated using the shown peaks. It was found that the crystal size of the commercially-obtained ZnO powder was ~24 nm in diameter, and that the crystal size of the primary nanoparticles of the hierarchically-structured ZnO powder was ~22 nm in diameter after 450 °C heat treatment.

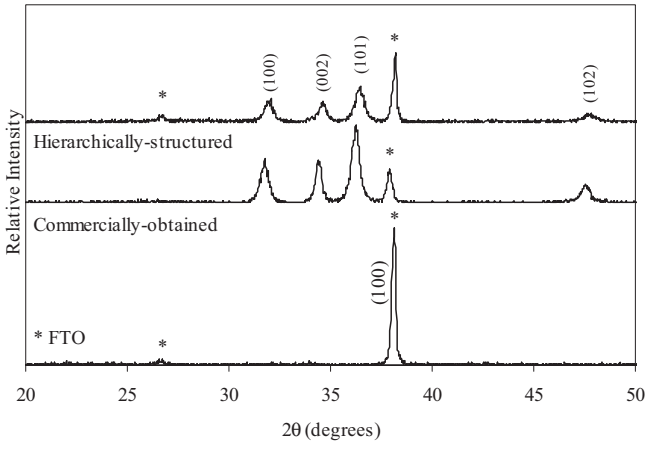

Figure 2. XRD peaks of ZnO films on FTO, comparing the peaks for hierarchically-structured ZnO and commercially-obtained ZnO particle powders after 450 °C heat treatment.

Additional SEM analysis was used to examine the morphology and to also estimate the crystal size of the secondary colloidal spheres in the hierarchically-structured ZnO film. In addition, SEM analysis was also performed on the commercially-obtained ZnO film for structural comparison. Figure 3

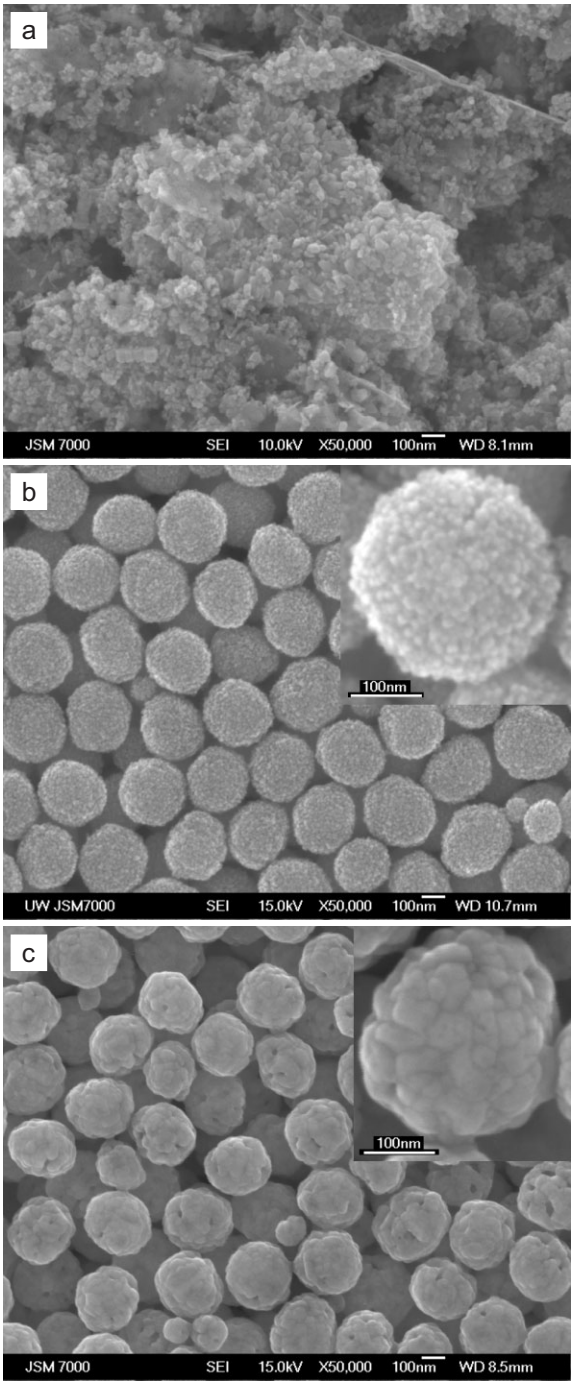

Figure 3. SEM images of a) commercially-obtained ZnO film after heat treatment at 450 °C, b) hierarchically-structured ZnO film before heat treatment, and c) hierarchically-structured ZnO film after 450 °C heat treatment. All SEM images are at 50 000× magnification. Both insets, each showing a single particle, are at 150 000× with a length bar scale of 100 nm.

ADVANCED MATERIALS

shows SEM images of the commercially-obtained ZnO particles after heat treatment, and the hierarchically-structured ZnO particles before and after heat treatment. It can be seen that the smaller particles ~24 nm in diameter in the commercially-obtained ZnO film are randomly agglomerated, forming a random network of much larger clusters. For the hierarchically-structured ZnO film, secondary colloidal spheres with a diameter between 200–250 nm were formed from numerous primary nanoparticles ~22 nm in diameter, as seen on the surface of the secondary spheres. The size of the primary nanoparticles was too small to conclusively determine the diameter from the SEM images; therefore, the crystal sizes obtained from the XRD results were used as the estimated diameters.

With additional 450 °C heat treatment performed on the hierarchically-structured ZnO film, the size of the secondary colloidal spheres slightly increased to a diameter estimated to be between 200–300 nm. Furthermore, it can be seen that the primary nanoparticles are also shown to be fused together with improved connectivity. It was observed that 450 °C was a sufficient sintering temperature for treating all the ZnO films for solar cell analysis. However, it was also observed that even with heat treatment, the particle packing was not close-packed, resulting in partial packing and numerous cracks in the film. This type of poor packing may have resulted in low interparticle connectivity between colloids, as shown in the SEM image, which may have influenced the solar cell performance of the film.

Solar cells consisting of films with hierarchically-structured ZnO particles were tested under illumination with 100 mW cm^{-2} intensity, and compared to films with commercially-available ZnO nanoparticles. Figure 4 compares the solar cell response and the absorption behavior of the hierarchically-structured ZnO film and the commercially-obtained ZnO film. Figure 4a shows the *I–V* characteristics of each solar cell consisting of 1) hierarchically-structured ZnO film sintered at 450 °C, and 2) commercially-obtained ZnO film also sintered at 450 °C. Table 1 summarizes the measured and calculated values obtained from each *I–V* curve in Figure 4a. It can be seen that the short-circuit current density and the overall light conversion efficiency of the ZnO film with hierarchical structure was higher than that of the ZnO film with commercially-obtained ZnO nanoparticles. One factor for the increase in short-circuit current density is the enhanced absorption behavior associated with the presence of large secondary colloidal spheres, resulting in higher photon absorption by way of light scattering, as shown in Figure 4b.

Table 1. Summary of the open-circuit voltage, short-circuit current density, maximum voltage and current output, fill factor, power output, and overall light conversion efficiency relative to the type of ZnO film.

ZnO Film	V_{oc} (mV)	J_{sc} (mA/cm^2)	V_{max} (mV)	J_{max} (mA/cm^2)	FF (%)	η (%)
Hierarchically -structured	670	10.9	420	8.35	48.1	3.51
Commercially -obtained	570	1.65	410	1.45	63.2	0.60

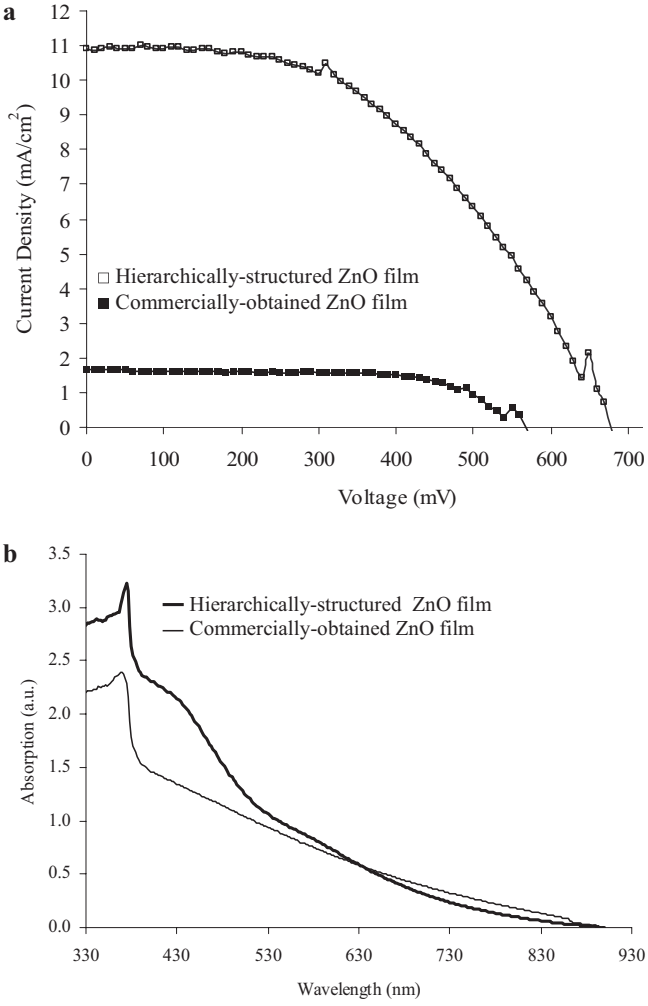

Figure 4. Plot of a) the *I–V* behavior of solar cells consisting of ZnO films, comparing the solar cell performance of hierarchically-structured ZnO film with that of dispersed ZnO film obtained commercially, and b) the absorption behavior of ZnO films on FTO, comparing the absorption peaks of hierarchically-structured ZnO film with that of dispersed ZnO film obtained commercially.

Figure 4b compares the variation in the absorption behavior of hierarchically-structured ZnO film with that of commercially-obtained ZnO film, normalized to the thickness of the films (3 μm). It can be seen that an absorption peak at ~390 nm is present for both films, representing the bandgap of ~3.2 eV, which is equivalent to the wavelength of ~387 nm. By comparing the absorption spectra of the two films, it can be seen that an additional absorption peak is shown at ~440 nm for the hierarchically-structured ZnO film, which is not seen for the commercially-obtained ZnO film. This additional absorption peak could be due to light scattering, caused by the presence of larger secondary colloidal spheres, which is in good agreement with the literature.[14,17] Typically, light scattering[18] occurs with particles >100 nm in diameter. Thus, with the presence of secondary spheres ~200–300 nm in diameter, the light scattering ability of the

larger spheres would enhance the ability of the hierarchically-structured ZnO film to absorb more of the photons, resulting in an increase in the generation of electron-hole pairs and an increase in the short-circuit current density, which is in accordance to previous reports.[13] The short-circuit current density for the hierarchically-structured ZnO film and for the commercially-obtained ZnO film were ~11 mA cm^{-2} and ~1.7 mA cm^{-2}, respectively. The short-circuit current density for the ZnO film with hierarchical structure was increased by ~9 mA cm^{-2}.

The open-circuit voltage was shown to be ~700 mV for the hierarchically-structured ZnO film and ~600 mV for the commercially-obtained ZnO film. This difference in the open-circuit voltage between the two types of film could be the result of different processing techniques used to fabricate the films, as the open-circuit voltage is dependent on the potential difference established by comparing the voltage of the film with that of the Pt counter electrode, where the surface chemistry of the ZnO material may influence the open-circuit voltage. Since the processing of the ZnO nanostructures are not optimized at this point, some deviation in the open-circuit voltage is expected. Furthermore, the fill factor for the hierarchically-structured ZnO film and the commercially-obtained ZnO film was shown to be ~48 % and ~68 %, respectively. The lower fill factor value associated with the hierarchically-structured ZnO film could be due to poor particle packing and cracking, as previously shown in the SEM images. The dispersed ZnO particles obtained commercially were also uniform in size ~24 nm in diameter; whereas, the hierarchically-structured ZnO particles obtained through chemical processing were shown to vary in size. The variation in particle size may have caused incomplete particle packing and cracking after sintering, which would result in low connectivity between particles.

Having a similar behavior as the short-circuit current density, a higher overall light conversion efficiency was also observed for the hierarchically-structured ZnO film, when compared to the commercially-obtained ZnO film. The overall light conversion efficiency for the hierarchically-structured and commercially-obtained ZnO films were ~0.6 % and ~3.5 %, respectively. This difference in the overall light conversion efficiency is expected since a similar difference was found for the short-circuit current density. A higher short-circuit current density would result in a higher overall light conversion efficiency since the overall light conversion efficiency is partly dependent on the short-circuit current density.

Since the commercially-obtained ZnO film mainly consists of ~24 nm diameter particles, the increase in the short-circuit current density and the overall light conversion efficiency shown in hierarchically-structured ZnO film was due to: 1) the hierarchical structure consisting of ~22 nm primary nanoparticles and ~200–300 nm secondary colloidal spheres, and 2) the light scattering effects of secondary colloidal spheres, resulting in more photon absorption and electron-hole generation.

In conclusion, it was found that ZnO film with hierarchical structure consisting of primary nanoparticles ~20 nm in diameter and secondary colloidal spheres ~200–300 nm in diameter resulted in a higher short-circuit current density of ~10.9 mA cm^{-2} and a higher overall efficiency of ~3.5 %, resulting in ~83 % improvement, as compared to the values obtained for commercially-obtained ZnO film. The increase in short-circuit current density by ~9.3 mA cm^{-2} and the increase in overall light conversion efficiency by ~2.9 % may have been due to the presence of larger secondary colloidal spheres. The presence of larger secondary spheres promotes enhanced light scattering for increased photon absorption.

Experimental

Zinc oxide (ZnO) colloidal solution was prepared from precursor materials by way of solvothermal processing. The chemicals used in making a colloidal solution of ZnO were zinc acetate (98 %, Alfa-Aesar, Ward Hill, MA), diethylene glycol (98 %, Sigma-Aldrich, St. Louis, MO), and deionized water (DI-H_2O). Commercially-available ZnO nanoparticles (99.99 %, Alfa-Aesar, Ward Hill, MA) were also obtained for comparison. Films were fabricated on fluorine-tin-oxide (FTO, TCO10-10, R_s ~10Ω/□, Solaronix SA, Switzerland) coated glass substrates.

The ZnO colloidal solution was prepared by hydrolyzing 0.01 mol of zinc acetate [$(CH_3CO_2)_2Zn$] in 100 mL diethylene glycol [$(HOCH_2CH_2)_2O$], as described by Jezequel et al. [11]. The reaction occurred when the mixed solution was heated under reflux to 160 °C for ~24 h. The as-synthesized solution was then placed in a centrifuge tube. The solution was centrifuged at a rate of ~1400 revolutions per minute (RPM) for ~5 h. After centrifugation, the precipitation of ZnO colloids segregated to the bottom of the tube. Part of the supernatant was removed and the colloids were then redispersed in ethanol by sonication for ~10 minutes. The resultant ZnO colloidal spheres were sealed and stored at room temperature. The colloidal spheres produced by this method have been reported to be monodispersed with a diameter size of ~300 nm, and consist of many primary nanoparticles with a diameter of ~20 nm.

To fabricate ZnO films, the conductive glass substrates were first hydrolyzed in boiling DI-H_2O at 90–100 °C for ~30 min and air-dried. Parallel edges of each substrate were covered with ~10 μm-thick scotch tape to control the thickness of the film. A few drops of the resultant ZnO colloidal spheres were then placed onto the glass substrates and the films were formed by a doctor-blading process. The films were then immediately heat treated at a temperature of 450 °C for 1 h, forming a layer of white film during the quick evaporation of the solvent. The thickness of the film was estimated to be ~10 μm, which is the same thickness as the spacers. The films consisting of commercially-obtained ZnO nanoparticles were also fabricated in the same manner, where the nanoparticles were also dispersed in ethanol.

Before solar cell testing, the ZnO films were heated to 70 °C and sensitized with standard ruthenium-based N3 red dye, cis-bis(iso-thiocyanato)bis(2,2′-bipyridyl-4,4′-di-carboxylato)ruthenium(II) (Solterra Fotovoltaico SA, Switzerland). The heated films were immersed in N3 dye with a concentration of ~5×10^{-4} M in ethanol for ~20 min. The samples were then rinsed with ethanol to remove excess dye on the surface and air-dried at room temperature.

Colloidal liquid silver (Ted Pella Inc., Redding, CA) was placed at the electrical contacts to improve the contact points and allowed to cure for 30 min at room temperature. Sheets of weigh paper ~30–40 μm thick were cut into small pieces ~1 mm × 4 mm in dimension and used as spacers. A spacer was placed at each edge of the ZnO film electrode and the counter electrode consisting of a platinum-coated silicon (Pt-Si) substrate with a Pt layer thickness of ~180 nm was placed on top, with the Pt-coated side of each Si substrate facing the ZnO film electrode. The two electrodes were then sandwiched together with two heavy duty clips.

ADVANCED MATERIALS

An iodide-based solution was used as the liquid electrolyte, consisting of 0.6 M tetra-butylammonium iodide (Sigma-Aldrich, St Louis, MO), 0.1 M lithium iodide (LiI, Sigma–Aldrich, St Louis, MO), 0.1 M iodine (I_2, Sigma–Aldrich, St Louis, MO), and 0.5 M 4-tert-butyl pyridine (Sigma–Aldrich, St Louis, MO) in acetonitrile (Mallinckrodt Baker, Phillipsburg, NJ). Right before analysis, drops of the liquid electrolyte were introduced to one edge of the sandwich, where capillary force was used to spread the liquid electrolyte in between the two electrodes. The light source was placed next to each solar cell device, allowing light to penetrate through the FTO back-contact to the ZnO film electrode with a constant light source intensity of ~ 100 mW cm^{-2}. A diagram of the solar cell device and the analysis setup is shown below.

X-Ray Diffraction (Philips PW1830 Diffractometer) and JADE software (MDI JADE 7 Materials Data XRD Pattern Processing, Identification, and Quantification) were used to verify the phase and crystal structure of the ZnO films. The diffractometer was set at 40 kV working voltage and 20 mA working ampere. All samples were scanned from 20–80° 2θ at a rate of 0.02 scans/second using X'Pert Industry Philips XRD software.

Scanning Electron Microscopy (JEOL JSM-5200, JEOL 840A, JSM-7000) was used to study the morphology of the ZnO particles and films. The samples were placed on an aluminum SEM stub, using either conductive carbon tape or a layer of silver paste for attachment. All samples were sputter-coated with a thin layer of Au/Pd or Pt prior to SEM observation. The images were obtained at 15 kV from 5000× up to 150 000× magnification, depending on the sample.

Optical absorption (Perkin Elmer Lambda 900 UV/VIS/IR Spectrometer) was used to analyze the absorption peaks of the ZnO films. The films prepared on FTO substrates were placed in the analysis chamber and scanned from 900 nm to 300 nm wavelengths using UV L900 WinLab software. The FTO substrates were used as the background sample.

Electrical characteristics and photovoltaic properties of each solar cell were measured using simulated AM1.5 sunlight illumination with 100 mW cm^{-2} light output. An Ultraviolet Solar Simulator (Model 16S, Solar Light Co., Philadelphia, PA) with a 200 W Xenon Lamp Power Supply (Model XPS 200, Solar Light Co., Philadelphia, PA) was used as the light source, and a Semiconductor Parameter Analyzer (4155A, Hewlett-Packard, Japan) was used to measure the current and voltage. The intensity of the light source provided by the Xenon lamp was measured with a Photometer/Radiometer (PMA2200, Solar Light Co., Philadelphia, PA) connected with a full spectrum Pyranometer (PMA2141, Solar Light Co., Philadelphia, PA).

The resulting current–voltage curves of the cells in the dark and as a function of incident light intensity (P_{source}) were used to derive the open-circuit voltage (V_{oc}) and the short-circuit current density (J_{sc}). A spot size of ~ 1 cm^2 was used in all measurements and was taken as the active area of each solar cell sample. All the current–voltage (I–V) measurements of the solar cells were obtained in the dark and under illumination, where a voltage range from –0.3 V to 2 V was used during each measurement. The I-V characteristics as a function of incident light intensity was used to obtain the open-circuit voltage (V_{oc}), short-circuit current density (J_{sc}), the maximum voltage point (V_{max}), and the maximum current density point (J_{max}). The values found from the I–V curves were then used to derive values for the fill factor (FF), the maximum power output density (P_{max}), and the overall power conversion efficiency (η) for each solar cell, using the following equations [1,3]:

$$FF\,(\%) = [(V_{max} \times J_{max}) / (V_{oc} \times J_{sc})] \times 100 \quad (1)$$

$$P_{max}\ (\mathrm{mW\,cm^{-2}}) = V_{max} \times J_{max} \quad (2)$$

$$\eta\,(\%) = [(FF \times V_{oc} \times J_{sc}) / P_{source}] \times 100 \quad (3)$$

Received: December 22, 2006
Revised: March 7, 2007
Published online: August 9, 2007

[1] a) M. A. Green, K. Emery, D. L. King, Y. Hishikawa, W. Warta, *Prog. Photovol.: Res. Appl.* **2006**, *14*, 455. b) A. Hagfeldt, M. Grätzel, *Acc. Chem. Res.* **2000**, *33*, 269. c) M. Grätzel, *J. Photochem. Photobiol. C* **2003**, *4*, 145.
[2] A. B. Kashyout, M. Soliman, M. El Gamal, M. Fathy, *Mater. Chem. Phys.* **2005**, *90*, 230.
[3] M. Grätzel, *Nature* **2001**, *414*, 338.
[4] E. M. Kaidashev, M. Lorenz, H. von Wenckstern, A. Rahm, H. C. Semmelhack, K. H. Han, G. Benndorf, C. Bundesmann, H. Hochmuth, M. Grundmann, *Appl. Phys. Lett.* **2003**, *82*, 3901.
[5] T. Dittrich, E. A. Lebedev, J. Weidmann, *Phys. Status Solidi A: RRN* **1998**, *165*, R5.
[6] a) K. Kakiuchi, E. Hosono, S. Fujihara, *J. Photochem. Photobiol. A* **2006**, *179*, 81. b) T. Zhang, W. Dong, M. Keeter-Brewer, K. Sanjit, R. N. Njabon, Z. R. Tian, *J. Am. Chem. Soc.*, in press.
[7] A. Hagfeldt, G. Boschloo, H. Lindström, E. Figgemeier, A. Holmberg, V. Aranyos, E. Magnusson, L. Malmqvist, *Coord. Chem. Rev.* **2004**, *248*, 1501.
[8] a) J. B. Baxter, E. S. Aydil, *Appl. Phys. Lett.* **2005**, *86*, 053 114. b) M. Law, L. E. Greene, J. C. Johnson, R. Saykally, P. Yang, *Nat. Mater.* **2005**, *4*, 455. c) J. B. Baxter, E. S. Aydil, *Sol. Energy Mater. Sol. Cells* **2006**, *90*, 607.
[9] a) K. Keis, C. Bauer, G. Boschloo, A. Hagfeldt, K. Westermark, H. Rensmo, H. Siegbahn, *J. Photochem. Photobiol. A* **2002**, *148*, 57. b) K. Keis, E. Magnusson, H. Lindstrom, S.-E. Lindquist, A. Hagfeldt, *Sol. Energy Mater. Sol. Cells* **2002**, *73*, 51.
[10] A. B. Kashyout, M. Soliman, M. El Gamal, M. Fathy, *Mater. Chem. Phys.* **2005**, *90*, 230.
[11] D. Jezequel, J. Guenot, N. Jouini, F. Fievet, *Mater. Sci. Forum* **1994**, *339*, 152.
[12] a) Z. S. Wang, H. Kawauchi, T. Kashima, H. Arakawa, *Coord. Chem. Rev.* **2004**, *248*, 1381. b) J. Ferber, J. Luther, *Sol. Energy Mater. Sol. Cells* **1998**, *54*, 265. c) Y. Tachibana, K. Hara, K. Sayama, H. Arakawa, *Chem. Mater.* **2002**, *14*, 2527. d) G. Rothenberger, P. Comte, M. Grätzel, *Sol. Energy Mater. Sol. Cells* **1999**, *58*, 321.
[13] a) S. Nishimura, N. Abrams, B. A. Lewis, L. I. Halaoui, T. E. Mallouk, K. D. Benkstein, J. van de Lagemaat, A. J. Frank, *J. Am. Chem. Soc.* **2003**, *125*, 6306. b) L. I. Halaoui, N. M. Abrams, T. E. Mallouk, *J. Phys. Chem. B* **2005**, *109*, 6334.
[14] J. C. Lytle, A. Stein, in *Annual Review of Nano Research*, Vol. 1 (Eds: G. Z. Cao, C. J. Brinker), World Scientific, Singapore China **2006**, Ch. 1.
[15] C. L. Huisman, J. Schoonman, A. Goosens, *Sol. Energy Mater. Sol. Cells* **2005**, *85*, 115.
[16] B. D. Cullity, *Elements of X-Ray Diffraction*, 2nd ed., Addison-Wesley, Massachusetts **1956**.
[17] Z. S. Wang, H. Kawauchi, T. Kashima, H. Arakawa, *Coord. Chem. Rev.* **2004**, *248*, 1381.
[18] G. Z. Cao, *Nanostructures & Nanomaterials: Synthesis, Properties, & Applications*, Imperial College, London **2004**.

